Spectro-consistent discretization of Navier-Stokes: a challenge to RANS and LES

R. W. C. P. VERSTAPPEN and A. E. P. VELDMAN
Department of Mathematics, University of Groningen, P.O. Box 800, 9700 AV Groningen, The Netherlands
(`verstappen@math.rug.nl`)

Abstract. In this paper, we discuss the results of a fourth-order, spectro-consistent discretization of the incompressible Navier-Stokes equations. In such an approach the discretization of a (skew-)symmetric operator is given by a (skew-)symmetric matrix. Numerical experiments with spectro-consistent discretizations and traditional methods are presented for a one-dimensional convection-diffusion equation. LES and RANS are challenged by giving a number of examples for which a fourth-order, spectro-consistent discretization of the Navier-Stokes equations *without any turbulence model* yields better (or at least equally good) results as large-eddy simulations or RANS computations, whereas the grids are comparable. The examples are taken from a number of recent workshops on complex turbulent flows.

Keywords: spatial discretization schemes, turbulent flows, DNS, LES, RANS.

1. Introduction

The costs of computing numerical solutions of the Navier-Stokes equations (Navier 1823, Stokes 1845) at high Reynolds numbers exceed the presently available computing resources. Richardsons verse 'Big whirls have little whirls, which feed on their velocity; and little whirls have smaller whirls, and so on to viscosity' hits off the situation well: most turbulent flows possess far more dynamically significant scales of motion than computers can process nowadays.

To get around this impossibility, turbulent flows are remodeled in such a way that the resulting physical description involves less scales of motion. Then, only a limited number of length and time scales need to be computed; the turbulence model takes care of the rest by describing its integral effect on the resolved scales. This decreases the costs of computing to an affordable level. Fewer scales, however, implies that the description is less accurate.

The continuous increase of computing power, as well as the sustained improvements of numerical methods, drive turbulent-flow simulations forwards. This evolution may clear the way by offering the possibility of computing more scales of motion and modeling less. Ultimately, this may bring us back to Navier and Stokes.

To solve more and more scales of motion, we need to push the algorithmic efficiency as far as it can get. In this paper, we evaluate the performance of a fourth-order, spectro-consistent discretization scheme for Navier-Stokes. In physical terms, we call a discretization of a convection-diffusion equation spectro-consistent when the discrete representation of convection redistributes energy over the scales of motion without dissipating it and the spatial discretization of diffusion dissipates energy from a scale without transporting energy to other scales of motion. From a mathematical point of view this means that the discretization of a

(skew-)symmetric differential operator is given by a (skew-)symmetric matrix or, in general, by a matrix which is spectrally equivalent to a (skew-)symmetric one. The reason to pursue these symmetry properties can be found in [1]: it preserves the stability of the underlying continuous operator and it yields smaller global truncation errors on nonuniform grids. In [1] second-order discretizations were considered. Here, higher-order discretizations will be discussed too.

In [2] we have proposed a fourth-order, spectro-consistent discretization of the incompressible Navier-Stokes equations. To make this paper self-contained, the main lines of this method will be sketched for a one-dimensional convection-diffusion equation (Section 2.1). In Section 2.2, we will show that the accuracy of second- and fourth-order spectro-consistent discretizations is better than that of traditional discretization methods that optimize the order of the local truncation error by means of a Lagrange interpolate. For this comparison we choose an exact solution of a steady convection-diffusion equation with a boundary-layer character. The results of the second- and fourth-order discretization are also compared to experimental data of a three-dimensional, turbulent flow in a lid-driven cavity at Reynolds number Re = 10,000 (Section 2.3).

In Sections 3 and 4, we challenge large-eddy simulations (LES) and Reynolds-averaged Navier-Stokes (RANS) compuations by giving a number of examples for which the fourth-order, spectro-consistent discretization of the Navier-Stokes equations *without any turbulence model* yields better (or at least equally good) results as large-eddy simulations or RANS computations, whereas the grids are comparable. The examples are taken from a number of recent workshops on complex turbulent flows. In all examples, low-order statistical quantities have been measured.

We will compare the results of LES with our method for a flow in a 3D lid-driven cavity at Re = 10,000 (Section 3.1) and for a flow past a long, square cylinder at Re = 22,000 (Section 3.2). Prasad and Koseff [3] have conducted a series of physical experiments in three-dimensional lid-driven cavities. The LES-data is taken from [4]. The flow past the square cylinder was selected as one of the test cases at two workshops on LES. See [5] and [6] for a discussion of the results. Lyn *et al.* [7] have measured this flow. Their experimental data (among others the Strouhal number, drag coefficient and velocity profiles at various locations in the flow) is available for comparison.

In Section 4, we challenge RANS by considering a fully developed turbulent flow in a channel with an array of surface-mounted cubes. The Reynolds number (based on channel width and bulk velocity) equals Re = 13,000. This flow was a test case at a workshop on refined flow modeling [8]. Mean velocity profiles as well as Reynolds stresses at various locations in the channel have been computed from the Reynolds-averaged Navier-Stokes equations by several groups. Meinders *et al.* [9] have measured mean velocities and Reynolds stresses for comparison.

2. Spectro-consistent discretization schemes

In this section we will discuss spectro-consistent spatial discretization methods for convection-diffusion equations. The first two sections deal with a one-dimensional convection-diffusion equation; the third section concerns a turbulent flow in three spatial dimensions.

2.1. CHOICE OF THE DISCRETIZATION

We will explain our choice of the discretization on nonuniform grids by studying the convection-diffusion equation

$$\frac{\partial \phi}{\partial t} + u \frac{\partial \phi}{\partial x} - k \frac{\partial^2 \phi}{\partial x^2} = 0.$$

This equation will be discretized in a finite-volume fashion (for notation see Figure 1). Such a discretization will result in an expression of the form

$$\boldsymbol{H} \frac{d\boldsymbol{\phi}_h}{dt} + \boldsymbol{M}\boldsymbol{\phi}_h = 0, \tag{1}$$

where $\boldsymbol{H}$ is a (positive-definite) diagonal matrix representing the size of the individual control volumes, whereas $\boldsymbol{M}$ is built from the flux contributions through the control faces.

The 'kinetic' energy of the discrete solution, defined by $||\boldsymbol{\phi}_h||_h^2 = \boldsymbol{\phi}_h^* \boldsymbol{H} \boldsymbol{\phi}_h$, evolves in time according to

$$\frac{d}{dt}||\boldsymbol{\phi}_h||_h^2 = \frac{d}{dt}(\boldsymbol{\phi}_h^* \boldsymbol{H} \boldsymbol{\phi}_h) = -\boldsymbol{\phi}_h^*(\boldsymbol{M} + \boldsymbol{M}^*)\boldsymbol{\phi}_h.$$

The right-hand side is negative for all $\boldsymbol{\phi} \neq \boldsymbol{0}$ if and only if the symmetric part of $\boldsymbol{M}$ is positive definite. This implies that the semi-discrete system (1) is stable under precisely this condition.

In the continuous case convection corresponds to a skew-symmetric operator, whereas diffusion leads to a symmetric positive-definite operator. In our spectro-consistent approach we want these properties to hold also in the discretized case. To obtain such a discretization the control faces are chosen halfway between the grid points. With a second-order flux in $x_{i+1/2}$ given by

$$u \frac{\phi_{i+1} + \phi_i}{2} - k \frac{\phi_{i+1} - \phi_i}{x_{i+1} - x_{i-1}},$$

the discrete convection-diffusion equation becomes

$$h_f \frac{d\phi_i}{dt} + \tfrac{1}{2}u(\phi_{i+1} - \phi_{i-1}) - k\left(\frac{\phi_{i+1} - \phi_i}{x_{i+1} - x_i} - \frac{\phi_{i-1} - \phi_i}{x_{i-1} - x_i}\right) = 0. \tag{2}$$

Manteuffel and White [10] have proven theoretically that, on grids where the ratio between the smallest and the largest mesh size is bounded during grid refinement, this method is second-order accurate in space. Practical experiences with this method have been presented by Veldman and Rinzema [1].

We will next turn this method into a fourth-order method. To that end we write down a similar equation on a two times larger control volume (see Figure 1)

$$h_c \frac{d\phi_i}{dt} + \tfrac{1}{2}u(\phi_{i+2} - \phi_{i-2}) - \text{diffusive terms} = 0. \tag{3}$$

The leading term in the discretization error can be removed through a Richardson extrapolation from (2) and (3). Since the errors in (2) and (3) are of third order, on a uniform grid this
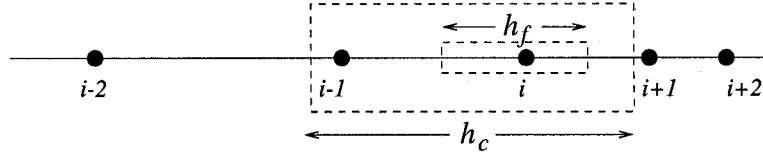
Figure 1. Fine (h_f) and coarse (h_c) control volumes. The control faces are located halfway the grid points ($i, i\pm1$) and ($i, i \pm 2$), respectively.

would mean to make a combination 8* (2)–(3). On a nonuniform grid one would be tempted to tune the weights to the actual mesh sizes, but we think it important that the skew-symmetry of the convective contribution is maintained. This can only be achieved when the weights are taken independent of the grid location, and hence equal to the uniform weights. In this way the discretization of the convective derivative becomes

$$H_i \frac{\partial \phi}{\partial x} \approx \tfrac{1}{2}(-\phi_{i+2} + 8\phi_{i+1} - 8\phi_{i-1} + \phi_{i-2}), \tag{4}$$

where

$$H_i = \tfrac{1}{2}(-x_{i+2} + 8x_{i+1} - 8x_{i-1} + x_{i-2}).$$

The diffusive term undergoes a similar treatment leading to

$$H_i \frac{\partial^2 \phi}{\partial x^2} \approx 8\left(\frac{\phi_{i+1} - \phi_i}{x_{i+1} - x_i} - \frac{\phi_{i-1} - \phi_i}{x_{i-1} - x_i}\right) - \left(\frac{\phi_{i+2} - \phi_i}{x_{i+2} - x_i} - \frac{\phi_{i-2} - \phi_i}{x_{i-2} - x_i}\right). \tag{5}$$

On a uniform grid we obtain, of course, the usual fourth-order method, but on nonuniform grids the method differs!

2.2. COMPARISON WITH TRADITIONAL DISCRETIZATION METHODS

We will demonstrate the performance of the above 2nd and 4th-order spectro-consistent methods by comparing them with the traditional discretization methods based on Lagrange interpolation (minimizing local truncation error). Since on uniform grids the methods are equal, we choose an example with a boundary-layer character, requiring grid refinement near the outflow boundary $x = 1$. Thus, we solve the steady convection-diffusion equation

$$\frac{\partial \phi}{\partial x} - k\frac{\partial^2 \phi}{\partial x^2} = 0 \ \ (0 < x < 1) \ \ \phi(0) = 0, \ \phi(1) = 1, \tag{6}$$

with a diffusion coefficient equal to $k = 0.001$.

Two types of grid have been examined. Firstly, we will present results for piecewise-uniform grids where the interval [0, 1] is split into two parts, in each of which the grid is taken uniform. The interface point, denoted by $1 - d$, is chosen near the edge of the boundary layer which has thickness $d = O(k)$. In both parts half of the grid points are positioned. Note that near the interface point the grid size abruptly changes, and only here the discretization differs from the Lagrangian one. Secondly, we have investigated more smoothly stretched grids. Results will be presented for a grid with a constant stretching (obtained through an exponential transformation function), again chosen such that half of the grid points lie in the boundary layer. Four discretization methods have been investigated:

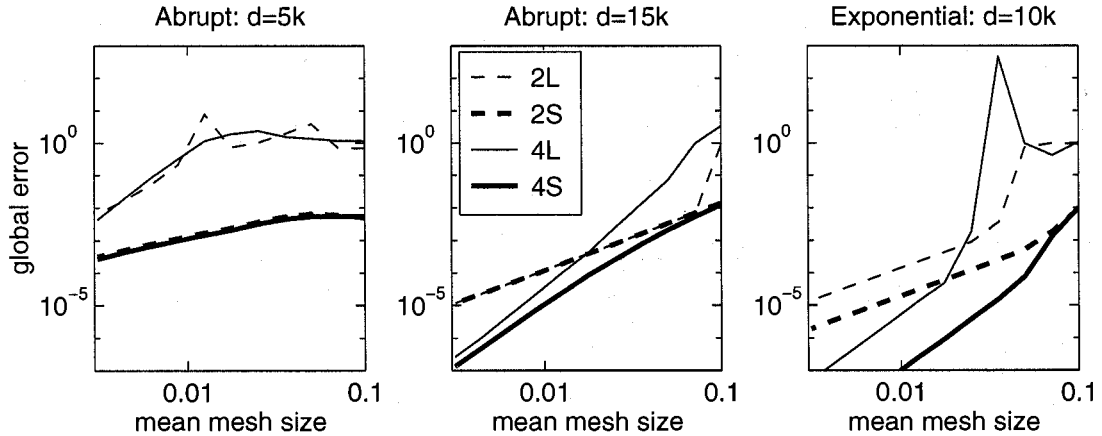– 2L: The traditional Lagrangian second-order method.

Figure 2. The global error as a function of the mean mesh size. Half of the grid points is located in the boundary layer of thickness *d*. Four methods are shown: 2L (second-order Lagrangian), 2S (second-order spectro-consistent), 4L (fourth-order Lagrangian with exact boundary conditions) and 4S (fourth-order spectro-consistent with second-order boundary treatment).

– 2S: The second-order spectro-consistent method defined by (2).
– 4L: The traditional fourth-order Lagrangian method where we have implemented exact boundary conditions to circumvent the problem of a difference molecule that is too large near the boundary. In this way the boundary treatment does not interfere with the internal discretization.
– 4S: The method defined by (4, 5) where we solve the problems due to the 'missing' boundary conditions by using the second-order discretization (2) in the end points.

As the analytical solution to (6) is known, we can monitor the global discretization error defined by $||\phi_h - \phi_{\text{exact}}||_h$ (where the norm is the kinetic energy norm defined above). In Figure 2 we present the global error as a function of the mean mesh size ($= 1/N$, where N is the number of grid points). Two abrupt grids have been chosen, one in which $d = 5k$, which is too narrow to catch the boundary layer accurately, and one with $d = 15k$. Further, one exponential grid is shown with $d = 10k$ (on a smoothly stretched grid the location of the interface point is less critical).

A number of observations can be made. Firstly, often the fourth-order Lagrangian method is not more accurate than its second-order counterpart, especially when the number of grid points is not abundant. This explains why thus far fourth-order discretization has not been very popular.

Secondly, when the number of grid points is low, Lagrangian discretization is much less accurate than spectro-consistent discretization. Also, on the narrow abrupt grid Lagrangian discretization suffers most. In contrast, the spectro-consistent discretization method behaves smoothly on all grids; even on the coarsest grids the error does not exceed 10^{-2}. In turbulent-flow simulations we will always be in the situation where we have to cope with limitations on the affordable number of grid points; hence methods that are less sensitive in this respect are preferable.

Thirdly, on the exponential grid the fourth-order Lagrangian method nearly breaks down for $N = 28$ where the stretching factor is 0·72 (which is not extreme). For this class of methods some eigenvalues of the coefficient matrix may be located in the left halfplane. Upon
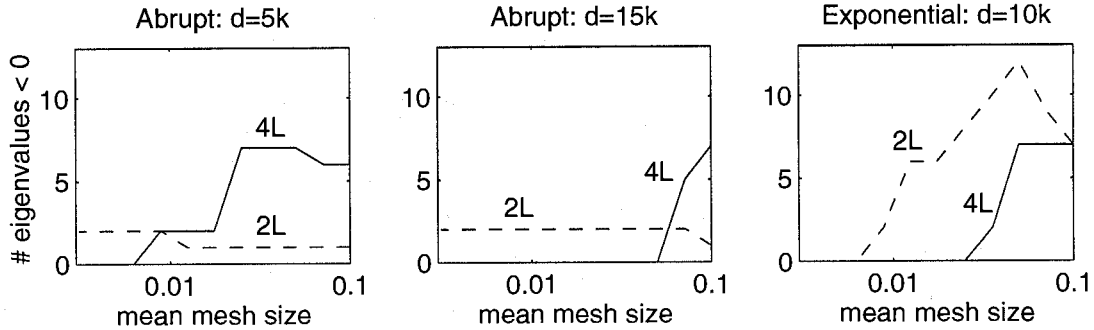
Figure 3. The number of eigenvalues of M located in the (unstable) left halfplane for the Lagrangian methods as a function of mean mesh size (2L second-order; 4L fourth-order with exact boundary conditions).

grid-refinement some of these eigenvalues will cross the imaginary axis, and, for this particular value of N, the system is (almost) singular. Note that the spectro-consistent fourth-order method for this value of N is already very accurate, with an error around 10^{-5}.

When one or more eigenvalues of the coefficient matrix H are located in the left halfplane, the semi-discrete system (1) is unstable, and cannot be integrated in the time domain; in the above examples we obtained the discrete solution by a direct matrix solver. To illustrate how serious this problem is, we present in Figure 3 the number of eigenvalues that are located in the unstable left halfplane. Only the Lagrangian methods are shown, since the spectro-consistent discretization always keeps the eigenvalues in the stable right halfplane.

2.3.   SECOND- VERSUS FOURTH-ORDER

Figure 2 shows that a fourth-order spectro-consistent method is more accurate than its second-order counterpart, in particular on the exponentially stretched grid. This implies that, given a certain required accuracy, the fourth-order method can be effective with fewer grid points used than for the second-order method. To verify that this also holds for a three-dimensional turbulent flow, we have compared the results of second- and fourth-order spectro-consistent methods for a direct numerical simulation of the flow in a cubical lid-driven cavity at Re = 10,000. Experimental results are available for comparison. The physical experiments of Prasad and Koseff [3] reveal that the flow in a cubical lid-driven cavity is unsteady at Re = 3,200. As the Reynolds number increases, the flow becomes more and more turbulent. At Re = 10,000, a power spectrum with a $-\frac{5}{3}$ slope has been observed. An analysis of driven-cavity flows by means of proper orthogonal decomposition can be found in [11].

The incompressible Navier-Stokes equations are discretized on a staggered grid, where the velocities and pressure are defined on the grid as proposed by Harlow and Welsh [12]. The convective and diffusive flux are integrated explicitly in time (2nd-order Adams-Bashforth), the pressure and the incompressibility constraint are treated implicitly. The time-discrete momentum equations are applied to control volumes. The spatial integrations are approximated by means of the midpoint rule. The convective term is discretized in such a manner that the corresponding coefficient matrix is skew-symmetric. The leading term of the local truncation error of the approximation consists of second-order terms. To eliminate the leading term of the truncation error, the momentum equations are also integrated over three times larger control volumes. The reason for taking three times larger control volumes – and not two times larger as in Section 2.1 – is illustrated in Figure 4: on a staggered grid, the control volumes for
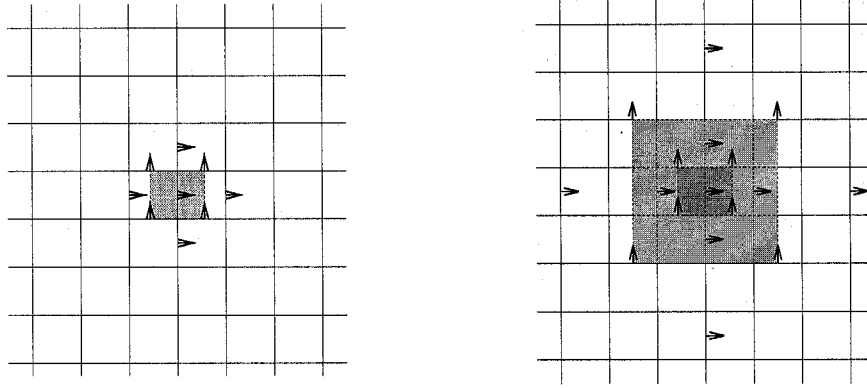
Figure 4. Control volumes for the second-order (left picture) and fourth-order (right) discretization of a horizontal component of the momentum equation. The arrows denote the velocities that are used to approximate the balance of momentum for the depicted control volumes.

horizontal components of the velocity are chosen in such a way that their corners coincide with positions of the vertical velocity. Three times larger volumes are the smallest ones possible with corners at these positions.

Since the truncation error in the integration of the momentum equations over the three times larger control volume is of the same form as the truncation error in the integration over the corresponding small control volume, we may eliminate the leading term of the truncation error and thus obtain a fourth-order method. As in Section 2.1 we use constant weights in the Richardson extrapolation on uniform and on nonuniform grids to preserve the symmetry properties of the underlying differential operators: the matrix that represents the discretization of a second-order derivative is symmetric; the discretization of a first-order derivative is skew-symmetric.

In the vicinity of boundaries, some three times larger control volumes do not fit into the flow domain. A misfit is treated as in Section 2.2: a second-order finite-volume discretization is used for misfitting parts. Obviously, we can also apply the balance of mass to three times larger control volumes and use these control volumes to eliminate the leading term in the truncation error in the discretization of the incompressibility constraint. Here, we do not follow that approach: we simply use the same control volumes for the balance of mass as in a second-order finite-volume method.

As is illustrated in Figure 5, the agreement between vertical mean velocities on the horizontal centerline in the symmetry plane of the cavity obtained with the fourth-order method on a stretched 50^3 grid (the grid spacing is exponentially stretched away from the wall; the largest mesh width is approximately seven times larger than the smallest) and the experiments is better than the agreement between the results of the second-order method on a 100^3 grid and the experiments.

In this example, the fourth-order results are more accurate than the second-order results, whereas the computational effort is about twenty times less. Indeed, the CPU-times per grid point and time step of both methods are comparable, a 50^3 grid has 8 times less grid points than a 100^3 grid, the time step (which is restricted by the CFL-condition) can be doubled, and the number of iterations needed to solve the pressure correction from the Poisson equation is somewhat less for a 50^3 grid than for a 100^3 grid: $8 \times 2 \times 1 \cdot 25 = 20$.
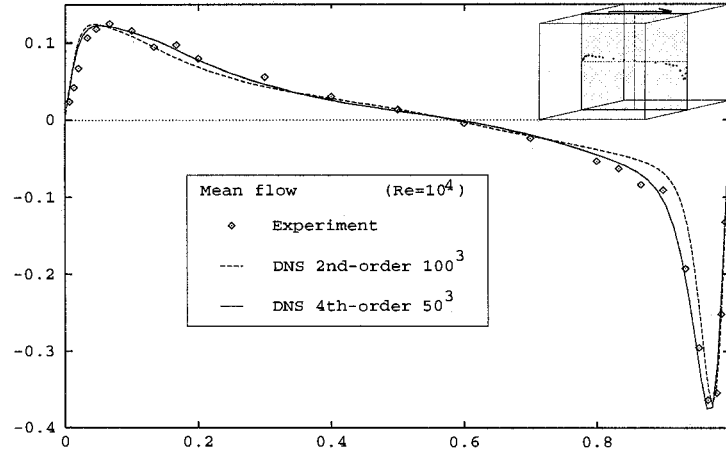
Figure 5. Second- and fourth-order DNS vs. experiment in a 3D driven cavity at Re $= 10,000$. The vertical mean velocity on the horizontal centerline in the symmetry plane of the cavity is shown.

3. Challenging LES

Both the algorithmic improvements and the improvements in computer performance have opened the door for us to solve the Navier-Stokes equations numerically for Reynolds numbers in the range $10^4 - 10^5$ without using any turbulence model. Results in this range will be compared to those of LES in this section. Section 3.1 deals with the flow in a lid-driven cavity at Re $= 10,000$; Section 3.2 concerns the flow past a long, square cylinder at Re $= 22,000$. In order to challenge LES, the spectro-consistent simulations have been performed on grids with mesh sizes that are comparable.

3.1. Flow in a 3D driven cavity at Re $= 10,000$

This section concerns the comparison with LES for a turbulent flow in a three-dimensional lid-driven cavity (Re $= 10,000$). Prasad and Koseff [3] have measured flows in cavities with different spanwise aspect ratios at Reynolds numbers (based on the length of the cavity and the speed at which the lid is driven) between 3,200 and 10,000. The LDA-measurements were performed along the horizontal and the vertical centre line in the symmetry plane of the cavity. The overall error in an instantaneous measured velocity is about 0·6%.

Zang *et al.* [4] have performed a number of large-eddy simulations of driven-cavity flows (with different aspect ratios and Reynolds numbers) and have compared their simulation results with the experimental data of Prasad and Koseff. The LES of Zang *et al.* uses a dynamic mixed subgrid-scale model. The subgrid model is incorporated in a finite-volume approach. The filtered Navier-Stokes equations are discretized on a non-staggered grid. A test-scale filter is introduced like in [13]. The test filtering volume is approximately twice as large as the grid filtering volume (in all spatial directions). The mixed model of Bardina *et al.* [14] forms the base model for the subgrid scales of motion. A fractional step method is employed for the semi-implicit time-marching procedure; the viscous terms, the pressure and the incompressibility constraint are treated implicitly. The discretization method is formally second-order accurate in both space and time.

We have performed a second- and a fourth-order accurate spectro-consistent simulation of a flow in a lid-driven cavity at Re $= 10,000$ with a spanwise aspect ratio of one half. The
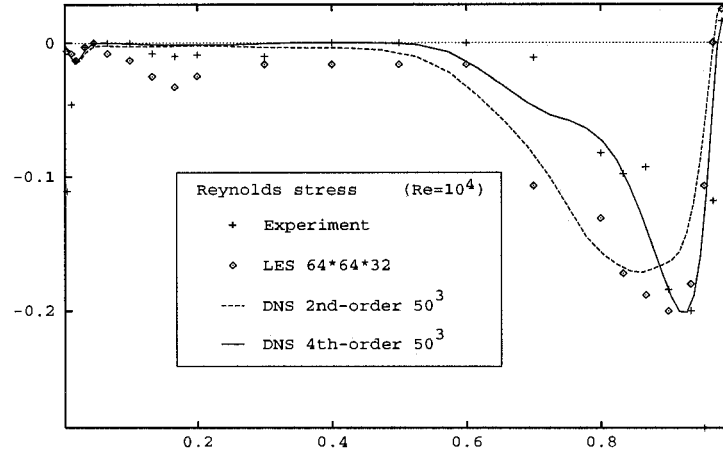
Figure 6. Comparison of experimental results, large-eddy and (second- and fourth-order) spectro-consistent simulation in a 3D driven cavity with aspect ratio 0·5 at Re $= 10,000$. The second-order LES uses approximately the same number of grid points as the second- and fourth-order simulations. The Reynolds stress $\overline{u'v'}$ along the vertical centre line in the central plane of the cavity (multiplied by 500) is shown. The LES-data is taken from [4]; the experimental data is taken from [3].

number of grid points is comparable to that of the LES of Zang *et al.*: the LES uses a stretched $64 \times 64 \times 32$ grid (131,072 grid points); here a stretched 50^3 grid (125,000 grid points) is used for both the second- and fourth-order simulation. It may be remarked that the grid used by the LES is somewhat more stretched. The smallest mesh size of the LES-grid is 5×10^{-3}; the first grid point of the 50^3 grid is located $7·65 \times 10^{-3}$ from the wall.

The agreement between the mean velocities of all simulations with the experimental data is good. The difference between mean velocities of the fourth-order simulation and the experiment falls within the estimation of error in the LDA-measurements. The agreement between the root-mean-square velocities is somewhat less. The LES underestimates the maximal values of the centre line root-mean-squares by up to 20% (see Figure 5 in [4]). The differences between the maximal root-mean-square velocities of the second- and fourth-order simulation and the experiment stay within 15% and 5%, respectively. The largest differences between the simulation methods occur in the Reynolds stresses at the centre lines. In Figure 6 we demonstrate the challenge of LES by comparing the Reynolds stress of the LES with that of the second- and fourth-order simulation and the experiment.

Figure 6 shows that the dynamic mixed subgrid-scale model used in the LES is still open for improvement: the Reynolds stress is systematically larger than in the experiment. It may be noted that the Reynolds stress of the LES is based on the velocities resolved by the grid, while the Reynolds stress that is computed from the experimental data contains contributions from all scales of motion, *i.e.* from the large scales as well as the small scales. Zang *et al.* [4] have estimated the contribution of the subgrid model to the Reynolds stress. They showed that this contribution is about an order of magnitude smaller than the resolved Reynolds stress, except in the vicinity of the lid, where it is of equal order. So, except in the vicinity of the lid, we need not to take the unresolved part of the Reynolds stress of the LES into account. Near the lid the subgrid contribution to the Reynolds stress has the wrong sign (see Figure 6 in [4]). Adding it to the resolved part worsens the agreement between the LES and the experiment.

From Figure 6 it is obvious that the second-order LES results do not lie nearer to the measurements than the second-order spectro-consistent simulation without model: the subgrid modeling does not improve the results significantly. Evidently, the fourth-order results are better than the second-order ones. The comparison between the LES and the fourth-order method turns out to favor the latter: the fourth-order method – not requiring any modeling and hence only containing numerical errors – shows a better performance.

3.2.   FLOW PAST A SQUARE CYLINDER AT RE = 22,000

The second comparison with LES concerns the flow past a long, square cylinder at Re = 22,000 (at zero angle of attack). We assume that the flow is periodical in the spanwise direction. The spanwise boundaries are taken four diameters apart. We prescribe laminar inflow at six and a half diameters upstream of the cylinder. Experiments by Lyn *et al.* [7] indicate a turbulence level (*i.e.* the ratio between the fluctuating and the mean velocity) of about 2% at four and a half diameters upstream from the cylinder. The lateral boundaries are taken 14 diameters apart. The outflow boundary is positioned at 20 diameters past the cylinder. In addition, in a buffer zone (of five diameters length) the Reynolds number is decreased from 22,000 to 1,000 to suppress (non-physical) waves which are reflected by the artificial outflow boundary. The (artificial) outflow conditions read $v_{nn} = w_{nn} = 0$ and $p_n =$ constant, where the constant is determined such that the mass inflow equals the mass outflow (at each time-step); this constant is approximately zero. No-slip boundaries are imposed at the surface of the cylinder.

We have used a $280 \times 210 \times 64$ staggered grid to cover the computational domain. The first grid point is spaced 0·005 from the cylinder surface. The grid is stretched out away from the cylinder surface by means of a sinh function; the ratio of the largest to smallest grid size in the streamwise direction is approximately 200. About 5% of the grid points are located in the buffer zone. The discrete Poisson equation for the pressure is solved with a combination of a Fast Fourier Transform method in the spanwise direction and a modified incomplete Choleski Conjugate-Gradient method in the resulting spectral space.

The start-up of the flow plus three shedding cycles have been computed on 16 nodes of a CRAY J932. We compute averages over three shedding cycles by sampling the flow at each time step. Velocities are also averaged over the top and bottom halves. All quantities are normalized by the cylinder width and the inflow velocity.

Table 1 shows the mean Strouhal number, the mean drag coefficient Cd, the mean lift coefficient Cl and the root-mean-square fluctuations of Cd and Cl. Here, it may be noted that the mean lift coefficient has not been measured; it should be zero by symmetry. All computed bulk quantities fall within the range set by the experiments, except for the root-mean-square of the fluctuations of the lift coefficient Cl which is slightly overestimated.

Figure 7 shows a comparison of mean streamwise velocities with experimental data at four locations past the cylinder. The agreement between the experimental data and the numerical data is good.

The flow past a square cylinder at Re = 22,000 (at zero angle of attack) has served as a test case at two LES workshops. The results submitted to the workshops can be found in [5] and [6]. The results show a great variation in the predictions, and it was concluded that this flow forms a major challenge to current LES techniques; no one has found the definite solution, yet. There is no doubt that the definite solution has to be computed by means of an accurate, cost-effective numerical method. In Figure 8, we have plotted the drag coefficients of almost

Table 1. Comparison with experiment: bulk quantities

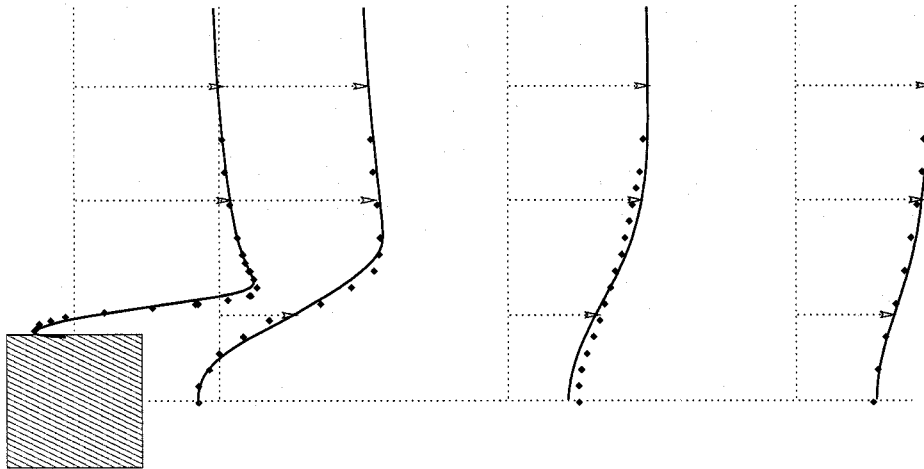|	Simulation	Lyn *et al.* [7]	Experiments Lee [15]	Vickery [16]
Mean Strouhal number	0·133	0·133 ± 0·003	—	—
Mean drag coefficient Cd	2·09	2·1	2·05	2·05
Mean lift coefficient Cl	0·005	—	—	—
Rms fluctuation of Cd	0·178	—	0·16 − 0·23	—
Rms fluctuation of Cl	1·45	—	0·68 − 1·32	—

Figure 7. A comparison of mean velocities of the fourth-order simulation with experimental results. The experimental data is taken from ERCOFTAC Database Case 43; see also Lyn *et al.* [7]. What is shown is the mean streamwise velocity. The continuous lines correspond to the simulation; the experimental data is depicted by the dots.

all the submissions versus the numerical method that has been applied. Here, we have left out a few, namely those that had serious failings (a too large lift coefficient, or a shedding frequency that differed significantly from the experiments).

There are of course many factors that (can) affect the prediction of the drag coefficient: the subgrid scale model, the value of parameters in the model, the grid resolution, the numerical approach, the treatment of the walls, etc. Unfortunately, these factors varied during the workshops, and consequently it is difficult to trace the source of the errors in the results of the simulations.

As can be seen in Figure 8, large-eddy simulations with a QUICK or a third-order upwind (U3) discretization predict a drag force which is too large. The U3-approach that comes closest to the experimental data uses approximately five times the number of grid points of each of the other QUICK/U3-methods. Although we cannot draw firm conclusions, for the reason mentioned above, it is most likely that the artificial diffusion added by QUICK/U3 contaminates the results.
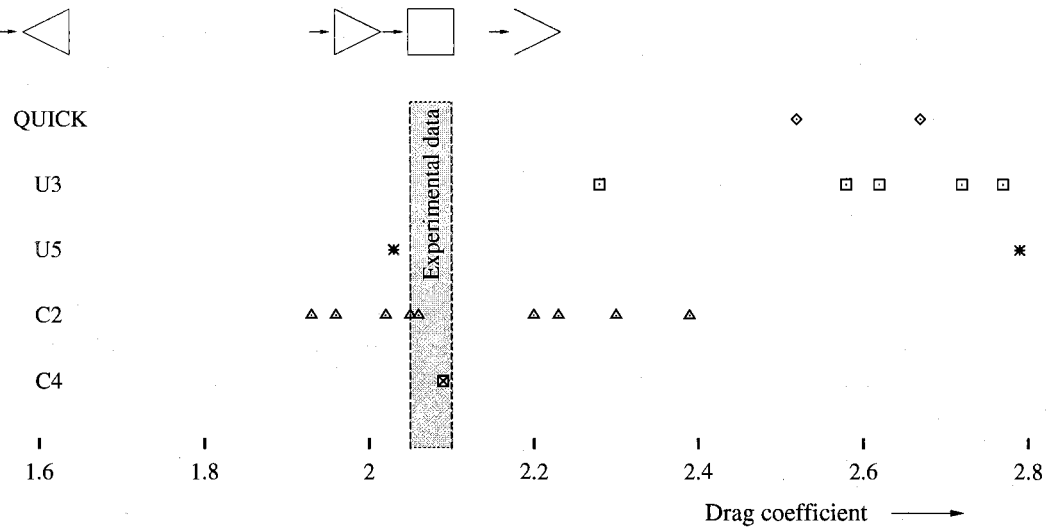
Figure 8. The mean drag coefficient versus the discretization of the convective terms of the Navier-Stokes equations. Here, U stands for upwind, and C for a central discretization. The number denotes the order of the method: C2, for example, represents a second-order central discretization. The experimental results of Lyn *et al.* [7], Lee [15] and Vickery [16] fall within the shaded area. The results of the large-eddy simulations are taken from [5] and [6]. The 2D shapes at the top are shown for comparison: the drag coefficient of the left wedge is about 1·6; the drag coefficient of the right half-open triangle is about 2·2. These values can, for instance, be found in [17, pp. 399].

The performance of subgrid models is difficult to judge since modelling errors and numerical errors interact; see also [18]. To separate these errors, a number of subgrid models need to be considered within the same numerical approach. We feel that spectro-consistent methods provide a good basis for evaluating turbulence models, since they are accurate on nonuniform grids and the character of the numerical error is well-defined: the error in the convective term is convective; the error in the diffusive term is diffusive.

4. Challenging RANS

A number of complicated physical phenomena, such as transition, separation, reattachment, and vortex shedding can be observed in turbulent flows past bluff bodies. Typically, the large-scale structures dominate the turbulent transport in these flows. This holds definitely for the flow past a square cylinder at Re = 22,000. Such flows are difficult to treat with RANS models. It is generally expected that LES offers a better approach for these types of flow, since it avoids the need to model the large eddies which strongly depend on the configuration. Yet, as remarked in [5], with properly chosen statistical models, RANS computations can simulate these flows at lower costs, but also at lower accuracy. The drag predictions of RANS models for the flow past a square cylinder at Re = 22,000, for example, vary from 1·637 (for $k - \epsilon$) to 2·43 (two-layer RSE).

In the remainder of this section we will compare the results of Reynolds-averaged and spectro-consistent Navier-Stokes computations for a fully developed flow in a two-dimensional channel with surface-mounted cubical obstacles. This flow has served as a test case for turbulence modeling at the 6th ERCOFTAC/IAHR/COST Workshop on Refined Flow Modelling which was held at Delft University of Technology in June 1997 [8].
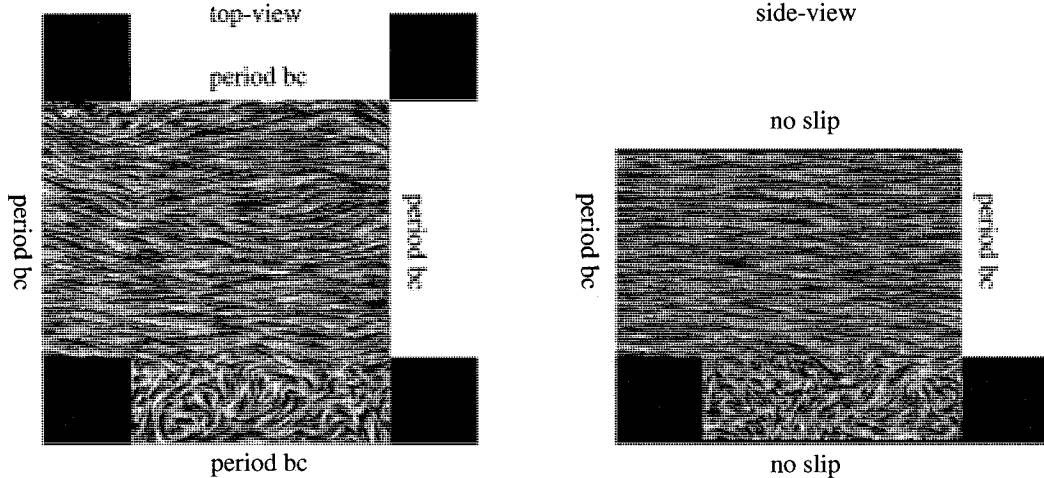
Figure 9. Top- and side-view of a sub-channel unit. An instantaneous flow field at two planes through the centre of the cubes is shown. This field results from the 100^3 DNS. In both pictures the flow is directed from left to right. The visualization has been made by means of the spot noise technique. For details on this technique the reader is referred to [19]. It may be noted that large structures of recirculating flow behind the obstacles are not present in any of the snapshots of this flow. These regions can only be observed if the flow is averaged over a long period in time.

4.1. FLOW IN A CHANNEL WITH SURFACE-MOUNTED CUBICAL OBSTACLES

The problem considered is the fully developed flow in a channel, where a matrix of 25×10 cubes is placed regularly at the bottom of the channel. The Reynolds number based on the width of the channel and the bulk velocity is equal to Re = 13,000. The channel is 3·4 times wider than a cube. The pitch of the cubes is four cube lengths in both the streamwise and the spanwise direction.

Meinders *et al.* [9] have measured this complex turbulent flow. Their flow measurements around the 18th row from the inlet showed that the influence of the in- and outlet can be neglected there. Hence, the computational domain for a numerical simulation can be confined to a sub-channel unit of dimension $4h \times 3\cdot4h \times 4h$ (where h denotes the height of a cube) with periodic boundary conditions in both the streamwise and the spanwise directions. Figure 9 displays the sub-channel unit.

Here, all quantities are normalized by the channel width and the bulk velocity. We have applied the fourth-order, spectro-consistent method that is outlined in Section 2 to compute mean velocity profiles and Reynolds stresses at various locations in the sub-channel. To this end, the sub-channel is covered by a 100^3 grid. The first mesh point is spaced 0·006 to a wall. A cube is represented by 40 grid points in each direction. The grid is slightly stretched: the largest grid size is approximately three times the smallest. No-slip boundaries are imposed at the surfaces of the cubical obstacles and also on the walls of the channel.

The convective and diffusive flux were integrated explicitly in time (by means of a one-leg method; see [2] for more details), the pressure gradient and the incompressibility constraint were integrated implicitly. In this case, the mass flow rate through the sub-channel is prescribed (such that the Reynolds number is kept constant at Re = 13,000). We satisfy this condition by computing a pressure drop Δp, which depends on time, but not on space. The pressure drop is computed at each time step, without iteration. To that end, the pressure p
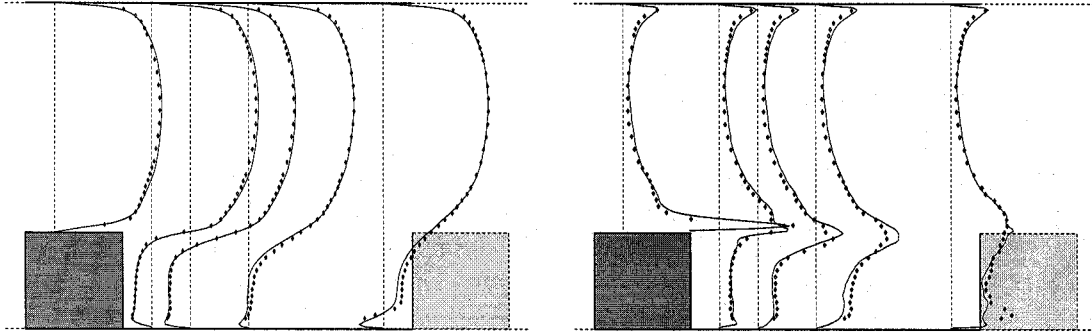
Figure 10. A comparison of first-order statistics and second-order statistics of the 100^3 simulation with experimental data. The left-hand picture displays the mean streamwise velocity $\overline{u}$ in the symmetry plane parallel to the streamwise direction that bisects a cube. The right-hand picture shows the mean-square of the fluctuating streamwise velocity $\overline{u'u'}$. The geometry is drawn to scale. The continuous lines correspond to the simulation; the experimental data is depicted by the dots.

is written as $p = q + \Delta p * s$, where q satisfies a Poisson equation with periodic boundary conditions in the streamwise direction, and the scalar s satisfies a Laplace equation, where s at the outflow boundary is one unit lower than s at the inflow. The part q of the pressure is computed every time step, namely in such a way that the divergence of the corresponding, discrete, velocity field is zero; the time-independent part s is computed only once (before the time integration starts, of course).

The entire computation (including start-up and sampling time) took about 100 hours on one vector-processor of a CRAY C90. Mean velocity profiles as well as Reynolds stresses at various locations in the channel have been computed. The sampling of data for the computation of the first- and second-order statistics of the flow started after a transitional period of 100 (non-dimensional) time units. The time-averages were computed over 200 time units and over the two symmetrical halves of the sub-channel unit. Samples were taken at each time step.

Figure 10 shows a comparison of the first- and second-order statistics of the 100^3 simulation with the experimental data of Meinders *et al.* [9] in the symmetry plane parallel to the streamwise direction that bisects a cube. The agreement between the experimental data and the numerical data is excellent.

In order to challenge RANS computations, we have also performed a simulation at a 60^3 grid. On this grid, a cube is represented by 30 grid points in each direction. The first grid point of the 60^3 grid lies approximately twice as far from the wall than the first grid point of the 100^3 grid. The coarse grid simulation takes about one tenth of the CPU-time of the fine grid simulation, among other things because the time step can be increased by a factor of about two. It goes without saying that the numerical methods that we have applied on the 60^3 grid are identical to those on the 100^3 grid.

There were four groups who presented results of their RANS computations of the flow in the channel with surface-mounted cubes at the sixth ERCOFTAC/IAHR/COST Workshop on Refined Flow Modelling. Here, we restrict ourselves to the RANS computation (of Dr S. Jansson from the Department of Fluid Mechanics of Vattenfall Entvecklung AB in Sweden) that agreed the best with the available experimental data. The results of this RANS computation as well as those of all the other submitted computations can be found in the proceedings of the

workshop [8]. It may be noted that there were no results of large-eddy simulations submitted to this workshop, nor have there been any reported elsewhere.

The best RANS result was based on a second-order, cell-centered, finite-volume method. It applied the SIMPLEC solution technique and a Rhie-and-Chow interpolation method. The QUICK scheme was used for the velocities and the turbulent quantities were integrated by means of a second-order accurate scheme with a Van Leer limiter. Periodic boundary conditions were applied in the streamwise direction; the period was taken equal to four cube lengths. Symmetry conditions were applied in the spanwise directions. The spanwise boundaries were taken two cube lengths apart. Dirichlet conditions were applied at the solid walls, except for the dissipation rate ϵ: the normal derivative of ϵ was put to zero at solid walls. The turbulence model consisted of a two-layer eddy-viscosity combined with a standard $k - \epsilon$ model. The transport equation for the dissipation rate ϵ was not solved in near-wall regions, but instead it was computed explicitly from a predicted length scale.

This RANS computation was performed on a stretched, orthogonal grid of 67 by 72 by 57 points in the streamwise, the normal and the spanwise direction, respectively. Except for the spanwise direction, the grid spacing of this RANS computation is slightly finer than that of our 60^3 simulation. In the spanwise direction, the average resolution of the RANS computation is about two times finer than the average resolution the 60^3 grid, due to the fact that the RANS computation uses symmetry conditions and therefore can restrict its spanwise computational domain to two cube lengths, while in our simulation periodic boundary conditions have been applied in the spanwise direction with a period of four cube lengths.

Mean streamwise velocities are compared in Figure 11. On a corresponding grid, the mean velocities computed from the Reynolds averaged Navier-Stokes equations agree less with the experimental data than the results of the spectro-consistent simulation. The velocity profiles of the RANS computation are much too smooth. In addition, the maxima of the velocities are located in the symmetry-plane between two cubes, which is in distinct disagreement with the experimental data.

Finally, it may be observed that the convergence of the spectro-consistent simulation upon grid refinement is plain: the results on the 100^3 grid are closer to the measurements than those of the 60^3 grid.

5. Conclusion

In this paper, we have discussed the results of spectro-consistent discretizations of the Navier-Stokes equations. In such an approach the discretization of a (skew-)symmetric operator is given by a (skew-)symmetric matrix. Numerical experiments with a one-dimensional convection-diffusion equation have shown that spectro-consistent discretizations yield better results on nonuniform grids than traditional methods that optimize the order of the local truncation error. To challenge RANS and LES we have compared their results with those of a fourth-order, spectro-consistent discretization of the Navier-Stokes equations (without a turbulence model) for a number of complex, turbulent flows that have served as test cases in a number of workshops to assess the current state of the art of RANS computations and large eddy simulations. The comparison with LES has been carried out for a turbulent flow in a driven cavity Re = 10,000) and for a turbulent flow past a long, square cylinder at Re = 22,000. The comparison with RANS was based on a turbulent flow in a channel with surface-mounted cubical obstacles Re = 13,000). The simulations based on a spectro-consistent discretization
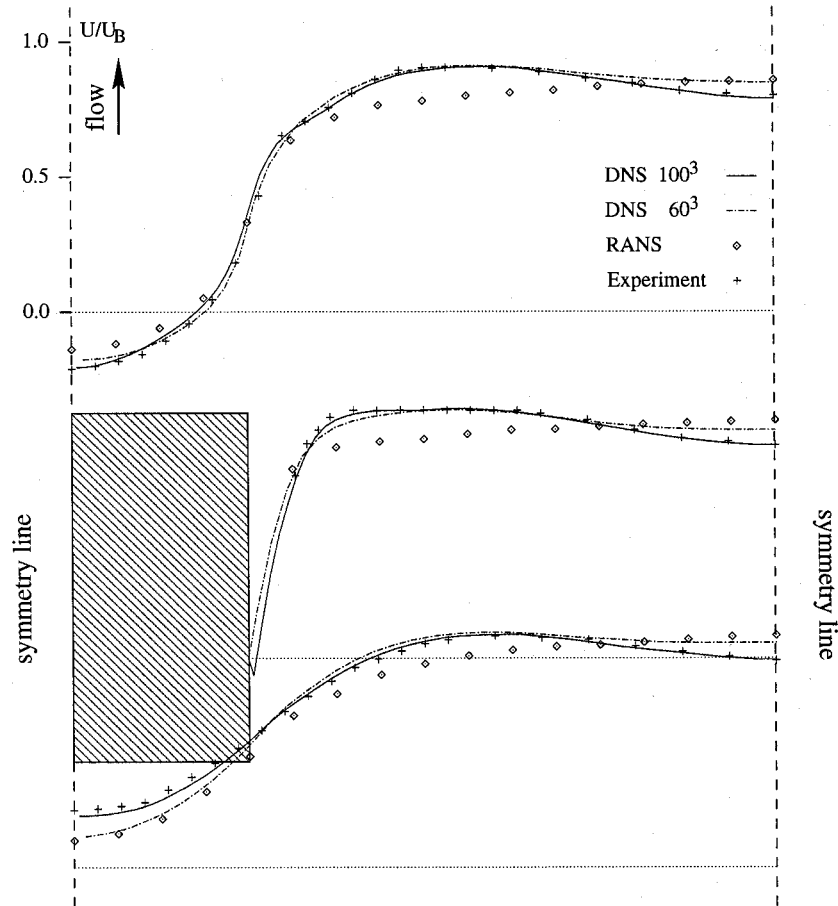
Figure 11. Comparison of the mean streamwise velocity at half cube height. The flow comes from below. The horizontal corresponds to the spanwise direction. The dashed vertical lines are lines of symmetry. The distance between them is two cube lengths. The lowermost profiles are located at 0·3 cube lengths before the front of the cube; the middlemost profiles are located at 0·3 cube lengths after the front. The uppermost profiles are located at one cube length after the middlemost. The velocity scale is shown for the uppermost profiles only; the other profiles have the same vertical scale. All velocities are normalized by the bulk velocity. The experimental data is taken from [9]; the RANS data is taken from [8].

of the incompressible Navier-Stokes equations – containing only numerical errors – can stand the comparison with RANS and LES in all cases that have been considered here. By challenging RANS and LES, we hope to give a strong impulse to the search for proper numerical schemes for turbulent-flow simulations.

Acknowledgements

References

1. A. E. P. Veldman and K. Rinzema, Playing with nonuniform grids. *J. Engng. Math.* 26 (1992) 119–130.
2. R. W. C. P. Verstappen and A. E. P. Veldman, Direct numerical simualtion of turbulence at lower costs. *J. Engng. Math.* 32 (1997) 143–159.
3. A. K. Prasad and J. R. Koseff, Reynolds number and end-wall effects on a lid-driven cavity flow. *Phys. Fluids A* 1 (1989) 208–218.
4. Y. Zang, R. L. Street and J. R. Koseff, A dynamic mixed subgrid-scale model and its application to turbulent recirculating flow. *Phys. Fluids A* 5 (1993) 3186–3196.
5. W. Rodi, J.H. Ferziger, M. Breuer and M. Pourquié, Status of Large Eddy Simulation: Results of a workshop. *ASME J. Fluids Eng.* 119 (1997) 248–262.
6. P. R. Voke, Flow past a square cylinder: test case LES2. In: J.P. Chollet *et al.* (eds.), *Direct and Large Eddy Simulation II* (1997) 355–373.
7. D. A. Lyn, S. Einav, W. Rodi and J. H. Park, A laser-Doppler-velocimetry study of emsemble-averaged characteristics of the turbulent near wake of a square cylinder. *J. Fluid Mech.* 304 (1995) 285–316.
8. K. Hanjalić and S. Obi (eds.), Proceedings 6th ERCOFTAC/IAHR/COST Workshop on Refined Flow Modeling, Vol. 3, Section Heat Transfer, Delft University of Technology, Delft (1997) 38 pp.
9. E. M. Meinders, K. Hanjalić, S. Obi and T. van der Meer, The flow in a matrix of cubical protrusions placed in a fully developed low Re number channel flow. Submitted.
10. T. A. Manteuffel and A. B. White Jr. The numerical solution of second-order boundary value problems on nonuniform meshes. *Mathematics of Computation* 47 (1986) 511–535.
11. W. Cazemier, R. W. C. P. Verstappen and A. E. P. Veldman, POD and low-dimensional models for driven cavity flows. Accepted for publication in *Phys. Fluids*.
12. F. H. Harlow and J. E. Welsh, Numerical calculation of time-dependent viscous incompressible flow of fluid with free surface. *Phys. Fluids* 8 (1965) 2182–2189.
13. M. Germano, U. Piomelli, P. Moin and W. H. Cabot, A dynamic subgrid-sacle eddy viscosity model. *Phys. Fluids A* 3 (1991) 1760–1765.
14. J. Bardina, J. F. Ferziger and W. C. Reynolds, Improved turbulence models based on LES of homogeneous incompressible turbulent flows. *Report No. TF-19*, Dept. of Mech. Engng., Stanford (1984).
15. B.E. Lee, The effect of turbulence on the surface pressure field of square prisms. *J. Fluid Mech.* 69 (1975) 263–282.
16. B. J. Vickery, Fluctuating lift and drag on a long square cylinder of square cross-section in a smooth and in a turbulent stream. *J. Fluid Mech.* 25 (1966) 481.
17. R. A. Granger, *Fluid Mechanics*. New York: CBS College Publishing (1985) 884 pp.
18. B. Vreman, B. Geurts and H. Keurten, Discretization error dominance over subgrid-terms in large eddy simulation of compressible shear layers in 2D. *Comm. Num. Meth. Eng.* 10 (1994) 785–790.
19. W. de Leeuw, *Presentation and Exploration of Flow Data*. Ph.D. Thesis, Delft University of Technology, Delft (1997) 107 pp.